LLNL-JRNL-2011275

Lawrence Livermore National Laboratory

Laser damage of crazed electron-beam high-reflectors following infrared and ultraviolet irradiation in the nanosecond pulse regime.

C Harthcock

September 2025

Applied Optics

Disclaimer

This work performed under the auspices of the U.S. Department of Energy by Lawrence Livermore National Laboratory under Contract DE-AC52-07NA27344.

Laser damage of crazed electron-beam high-reflectors following infrared and ultraviolet irradiation in the nanosecond pulse regime.

Colin Harthcock[1*], Amira Guediche[1], Saaxewer Diop[1], Christopher J. Stolz[1], Raluca Negres[1], Gener Gatmaitan[1], Rebeca Rangel[1], Frank Pan[1], Jian-Gang Weng[1], Andrew Lange[2], Rebecca Dylla-Spears[1]

[1]Lawrence Livermore National Laboratory; 7000 East Ave, Livermore CA, 94550
[2]Blue Origin, LLC; 21218 76th Ave S. Kent WA, 98032
[*]Harthcock1@llnl.gov

Abstract

Laser damage of optical components can be a limiting factor in scaling the energetics of high-peak and average power laser systems. Specifically for optical coatings, damage under nanosecond pulsed irradiation is initiated by pre-existing defects in the coating layers, including those that cause discontinuities in the structure like craze lines. Crazing or cracking in a multilayer dielectric optical coating is induced when the overall coating stress is sufficiently tensile and is an occasionally observed issue when employing more porous deposition techniques like electron-beam evaporation. In this study, electron-beam high-reflectors were fabricated utilizing process parameters that are known to induce crazing based on prior processing history to systematically evaluate the impact of crazing on reflector damage performance for 1064 nm and 355 nm lasers. The crazing that was observed were apparently nucleated at nodular defects. When the cross section of these nodules was investigated, it was observed that there were cracks into the fused silica substrate of approximately 5 μm in depth. The craze lines were irradiated with 1064 and 355 nm light at fluences slightly above the onset damage initiation fluence of the coating. The 1064 nm irradiated sub apertures exhibit laser damage but with no spatial correlation with the craze line, however the 355 nm irradiated area exhibited many damage sites along the craze line. Finite-difference time-domain electric field simulations were conducted and ~2x field amplification in hafnia was observed for the 355 nm wavelength case. The laser damage can be attributed to a slight electric field intensification coincidental with an area where UV damage-prone precursors are known to occur. The 355 nm laser damage in uncoated fused silica substrates have been previously correlated to initiate through localized UV absorption at the broken silica bonds in the tips of fractures.

1. Introduction

Crazing can occur in multilayer coating materials when the tensile stress exceeds the fracture toughness of the optical materials. Crazing typically occurs in lower energetic, thin film deposition techniques such as electron beam deposition or resistive heating evaporation. Crazing is more prevalent in coatings manufactured with fluoride materials but can also occur in oxide materials depending on the deposition parameters. Crazing risk also tends to increase in likelihood with increased film thickness or reduced humidity in the operating environment, like those found in a vacuum environment for instance. Attempts to reduce tensile stress in multilayer coatings deposited by electron beam have included using more energetic deposition methods such as ion-assisted deposition (IAD) or plasma ion-assisted deposition (PIAD) to increase the coating density via momentum transfer.[1] For multilayers deposited by electron beam without any extra energetic deposition methods, crazing can be mitigated by process modifications such as reduced O_2 flow rate during deposition,[2] and exploiting the coefficient of thermal expansion differences of the coating and substrate materials either by higher deposition temperatures or the use of substrate materials with higher thermal expansion than the coating materials.[3, 4]

Electric field intensification is an important metric to understand laser damage risk and Nikolai Bloembergen is attributed to the early development of electric field enhancement theory due to cracks in transparent dielectrics.[5] With advances in computers and Finite-Difference Time-Domain (FDTD) software, François Génin et al. modeled electric field intensification enhancements as high as 20x in cracks in bare fused silica surfaces at 351 nm.[6] There is a gap in the scientific literature corresponding to electric field intensification due to craze lines in multilayer high reflective coatings and this study attempts to understand why craze lines do not impact 1064 nm laser resistance, but do limit the 355 nm laser resistance of multilayer high reflective coatings.

For many of the near infrared (IR) petawatt class lasers using pulse compression gratings,[7] crazing lines in multilayer mirrors tend to be fairly resistant to laser exposure.[8-12] Although crazing lines do lead to scatter which can lead to beam modulation and downstream laser damage.[13, 14] High fluence, ultraviolet (UV) transport mirrors have been a goal for the laser fusion community for decades sparking research into wide bandgap fluoride coating materials.[15-20] However, this research was discontinued in the 1990's due to excessive tensile stress and the

associated craze lines that limited laser damage resistance. This has been a considerable limiting factor for UV-driven ICF configurations, such as the OMEGA laser at LLE and should be carefully considered for on-going and future efforts like those proposed at Xcimer.[21, 22] It is also of vital importance for NIF-like ICF designs, where the last two turning mirrors can be irradiated with high-intensity UV from target-induced backscatter.[23]

This study aims at increasing the community understanding of the impact of craze lines in multilayer mirror coatings as a function of wavelength to reconcile these observations between large-aperture NIR and UV laser systems. A secondary focus of this study is to improve understanding of how craze lines initiate, and the associated necessary stress levels needed to initiate craze lines. Mechanical stress-induced cracking has been determined as a contributing mechanism to nodule-induced laser damage,[24] and to our knowledge, this paper documents the first of its kind observation of substrate cracking under nodular defects and craze lines. We study the infrared and ultraviolet (UV) laser damage performance of multilayer dielectric coatings in the vicinity of craze lines, with the ultraviolet wavelength light initiating laser damage on the craze line. This observation is further bolstered by the large body of work linking UV laser damage to sub-surface cracks in bulk dielectric materials via UV absorption at the broken silica bonds at the tips of cracks[25-28] and likely correlates with a 2x electric field amplification in the vicinity of craze lines as simulated by finite-difference time-domain simulations in this study.

2. Experimental methods

High-reflector coatings were fabricated via electron-beam evaporation using silica as a low refractive index material and hafnia as a high refractive index material. The high-reflector was produced via periodic layering of quarter-wave optical thickness with a design of Substrate|$(HL)^{17}$HLL centered at 1064 nm and at 0 degrees angle of incidence. A quarter-wave of optical thickness of silica is denoted by “L” and a quarter-wave of hafnia is denoted by “H”. The coating was designed using OptiLayer, with layer materials and thicknesses optimized based on optical constants for the specific coating system prior to deposition. The standing electric field for the design was simulated via Optilayer software package at 1064 and 355 nm for near-normal incidence can be found in Fig. 1(a). All finite-difference time-domain electric field simulations were conducted using the Lumerical 2024 R2 FDTD analysis tool.

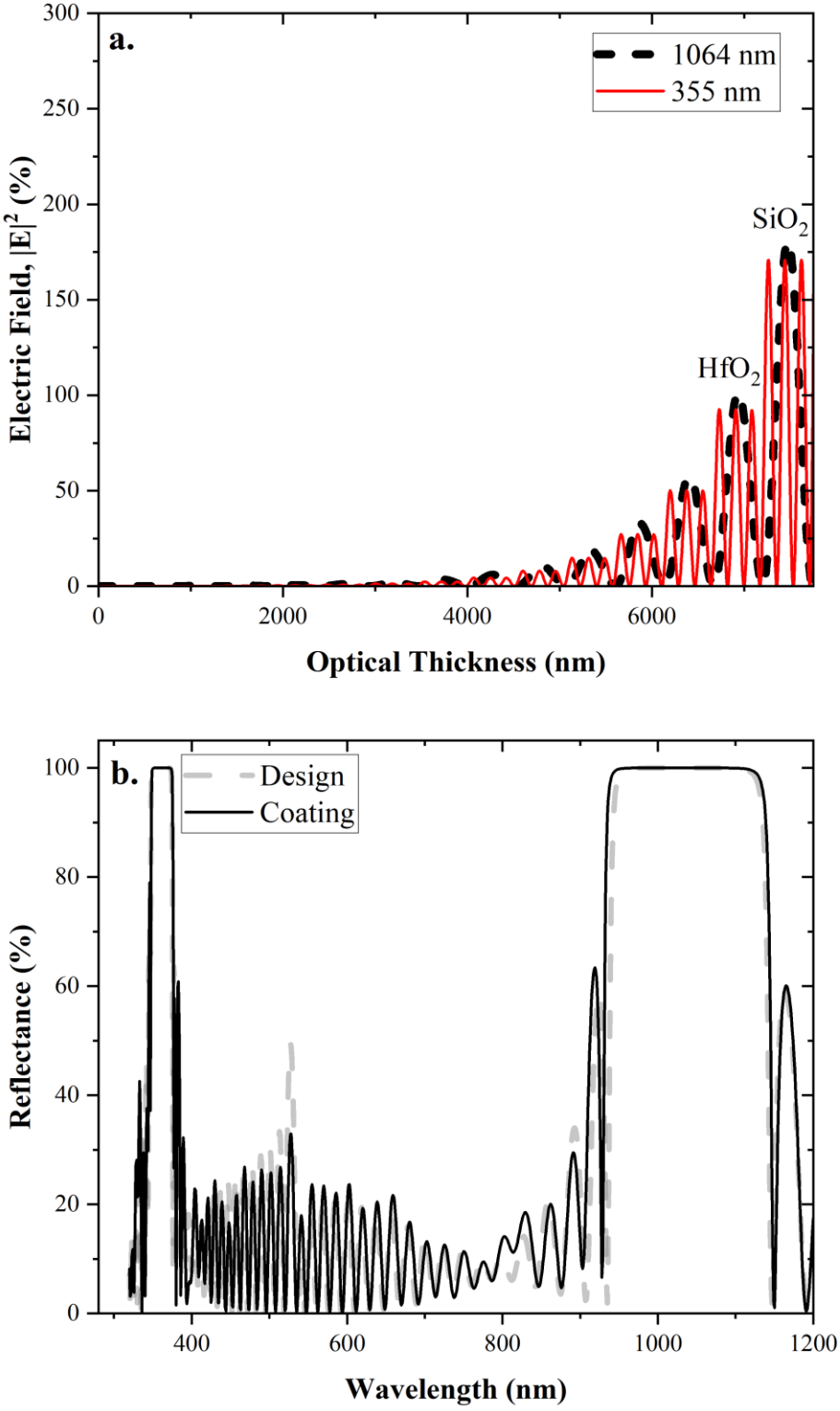
a.
1064 nm
355 nm
SiO2
HfO2
Electric Field, |E|2 (%)
Optical Thickness (nm)
0
50
100
150
200
250
300
0
2000
4000
6000
b.
Design
Coating
Reflectance (%)
Wavelength (nm)
0
20
40
60
80
100
400
600
800
1000
1200

Fig. 1. (a) The simulated electric field at normal incidence for 1064 nm and 355 nm wavelengths and (b) the spectral performance of the dielectric coating compared to the theoretical design.

Optical coatings were deposited using electron-beam evaporation in a coating system with a dual-planetary rotation using specific process parameters that have previously been seen to exhibit subtle crazing in similar samples. Two-inch diameter, 9.5 mm thick Corning 7980 0A fused silica substrates were prepared via ultrasonic JST cleaning. JST cleaning is a wet cleaning process utilizing ultrasonic agitation and involves solvents as well as numerous deionized water rinses which has been shown to successfully remove organic and inorganic defects from the substrate.[29] Prior to coating, the substrates were inspected to ensure better than 10/5 scratch/dig surface quality per MIL-PRF-13830B. The system was exposed to an extended thermal soak at 160 °C, with a base pressure of 1.00×10^{-5} Torr. This deposition temperature was chosen specifically because it has been historically shown to induce subtle crazing in hafnia silica-based multilayer dielectric (MLD) high-reflectors (HRs) for the two-inch aperture. This system uses a Temescal CV-12SLX power supply with a closed-loop feedback mechanism to continuously monitor rate and adjust power, compensating for any rate deviations. The viable testing real estate is known as the clear aperture and in this case, it is 95% of the full two-inch optical surface.

The resultant coating was inspected prior to laser irradiation. The spectral characteristics for the MLD coating were measured with an Agilent Cary 7000 Universal Measurement Spectrophotometer (UMS). The reflectance for both 1064 and 355 nm was greater than 99.9%, and the spectra was in excellent agreement with the coating design as reported in Fig. 1(b). When reverse engineering the resultant coating, the electric field was modeled to be within 5% of the theoretical design as reported in Fig. 1(a). Samples were inspected visually via bright light inspection per MIL-PRF-13830B as well as using a Keyence laser confocal microscope. The cross-sectional details of the nodular defect and surrounding craze line were investigated via gallium-focused ion-beam milling and scanning electron microscopy (SEM) using a FEI Helios 650 dual-beam instrument with an electron energy-dispersive spectrometer (EDS). A conductive platinum layer was coated on the sample to improve the signal-to-noise ratio and to protect the specimen during the FIB milling process. All pre-laser damage sample preparation and microscopy were conducted at EAG Eurofins under the guidance of the authors. The coating stress was determined by observation of coating-induced deformation of the substrate via reflected wavefront as observed on a Zygo Verifire GPI XP

HR four-inch interferometer utilizing a 1053 nm wavelength diode and collected at normal angle of incidence.

The laser damage performance of the films was evaluated by conducting laser damage testing via a raster test protocol using the first and third harmonic of an Nd:YAG laser system. The laser was operated in a single-longitudinal mode (Quanta-Ray Model PRO-350-10, Spectra-Physics, Inc, injection seeded) with a pulse duration of 8 ns (FWHM) and a near Gaussian temporal profile. All tests were performed at normal incidence and linearly polarized light. In all cases the sample was rotated such that the electric field was parallel to the direction of the craze. This polarization condition is often referred to as the transverse electric (T_E) polarization condition and will referred to in this manner from here on. The other polarization state is transverse magnetic (T_M) and was not experimentally explored in this study but has been included in simulation efforts for completeness. The near Gaussian laser beam diameter is formatted to 600 μm at $1/e^2$ maximum intensity for both wavelengths. Testing was conducted using 1 mm^2 raster scans like the ubiquitous MEL-01-013-0E raster standard on the craze line. A diagnostic reference arm was used to record the laser energy and spatial beam profile at an equivalent sample plane on each shot. In-situ optical microscopy with an approximate resolution of 1 μm was used to collect images before and after laser irradiation to detect any laser-induced surface modifications. In all cases the sample was first tested with UV irradiation then irradiated with IR light on a different craze line which was a minimum of 1 cm of separation on the optical surface. The sub-aperture tested via IR light was above the UV sub-aperture to ensure that gravity doesn't contaminate the IR sampled region. The overall fluence error is approximately 10-15% and includes the energy meter and beam profile measurement uncertainties.

3. Results and discussion

3.1 SEM and cross-sectional observations of a nodule-induced craze line

Following the visual inspection of the pristine coated but unirradiated samples, nodules were observed on the surfaces (Fig. 2) under high-intensity light. Some, but not all, of those nodules also had observable craze lines. There were no observed craze lines without the existence of a nodule. When inspected via SEM, the craze lines were observed to be 50~100 nm wide, terminating at the edge of the clear aperture and in all cases have a nodular defect somewhere along the line. A representative micrograph of a nodule and craze line are shown in Fig. 2(a, b) respectively. These

craze lines appear to originate at the nodular defect and radiate outward to the clear aperture of the coating, typically in a characteristic “horseshoe” shape. On the two-inch diameter optical surface, five craze lines are observed on the optical face. This nodule shown in Fig. 2a was examined using the FIB-SEM technique at two locations (Fig. 3 and 4) in areas close to both ends of the nodule using FIB and SEM.

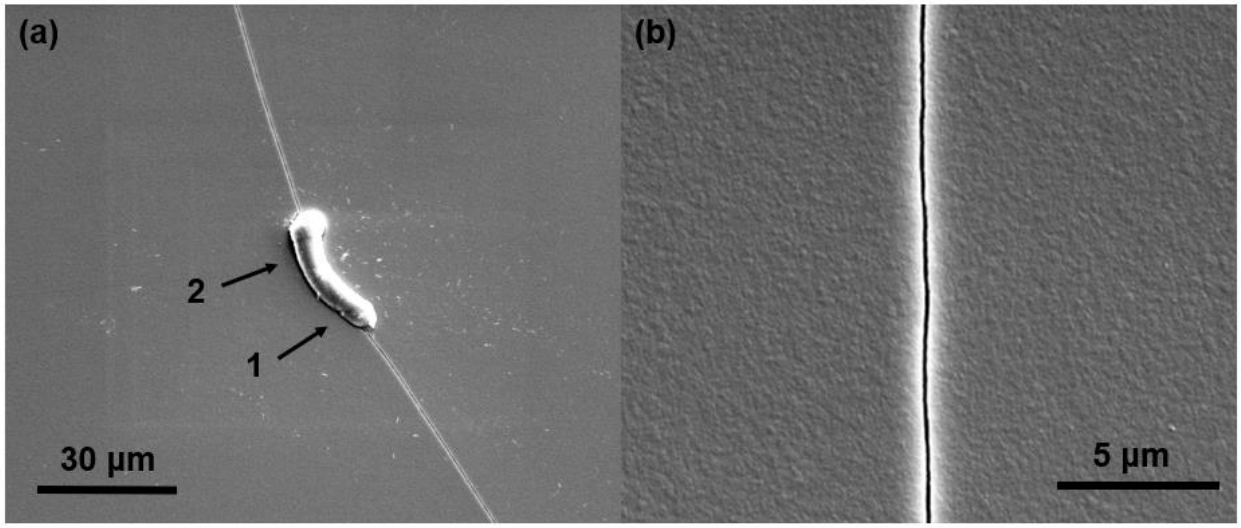

Fig. 2. (a) A typical nodule and associated craze line. The arrows with numbers correspond to the locations of FIB cross sections. (b) A close-up micrograph of the craze line.

Cross sectional views of the nodule were taken in two areas and are shown in Fig. 3. Electron energy-dispersive spectroscopy (EDS) analysis showed that the defect that initiated the nodule was dielectric in nature, likely attributed to flaking during the deposition process. It is notable that in both micrographs there is a crack initiating at the nodule and propagating into the substrate.

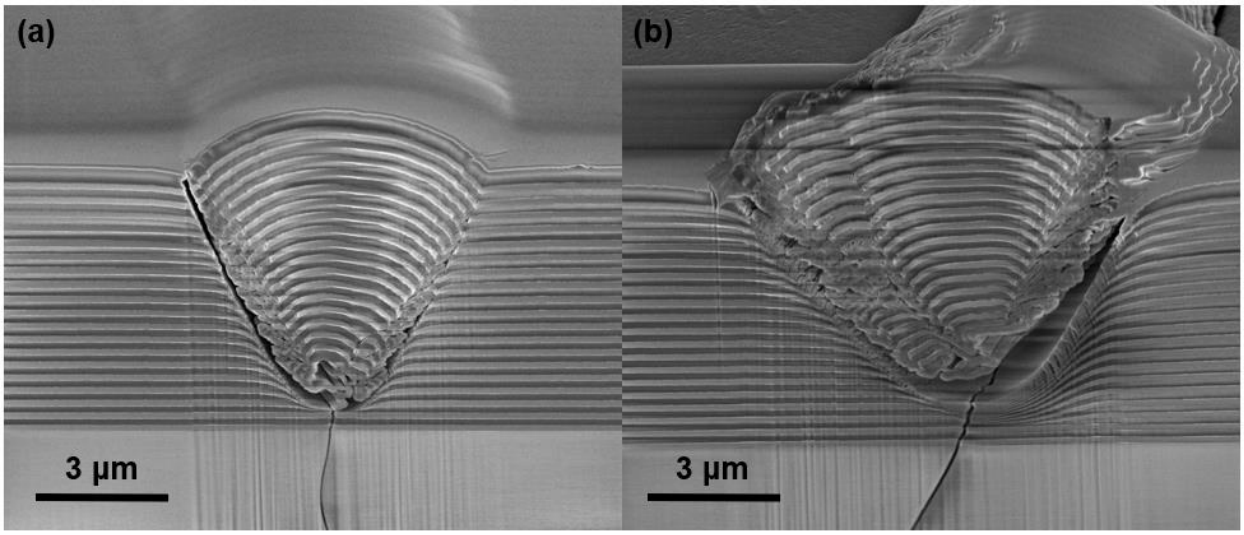

Fig. 3. FIB-SEM micrographs of the nodular defect at (a) location "1" in Fig. 2(a) and (b) location "2" in Fig. 2(a).

Fig. 4a and b shows the FIB-SEM micrograph images of the observed crack below Fig. 3a and b respectively. Fig. 4(a) corresponds to a FIB cut to the area denoted by "1" in Fig. 2(a) and Fig. 4(b) corresponds to a FIB cut to the area denoted by "2" in Fig. 2(a). In both locations there is a crack that propagates from the terminus of the nodular defect into the fused silica substrate which is approximately 5 µm long and 100 nm wide. It can also be observed from Fig. 4(a) that the nodule may have been introduced during the deposition of the fourth layer.

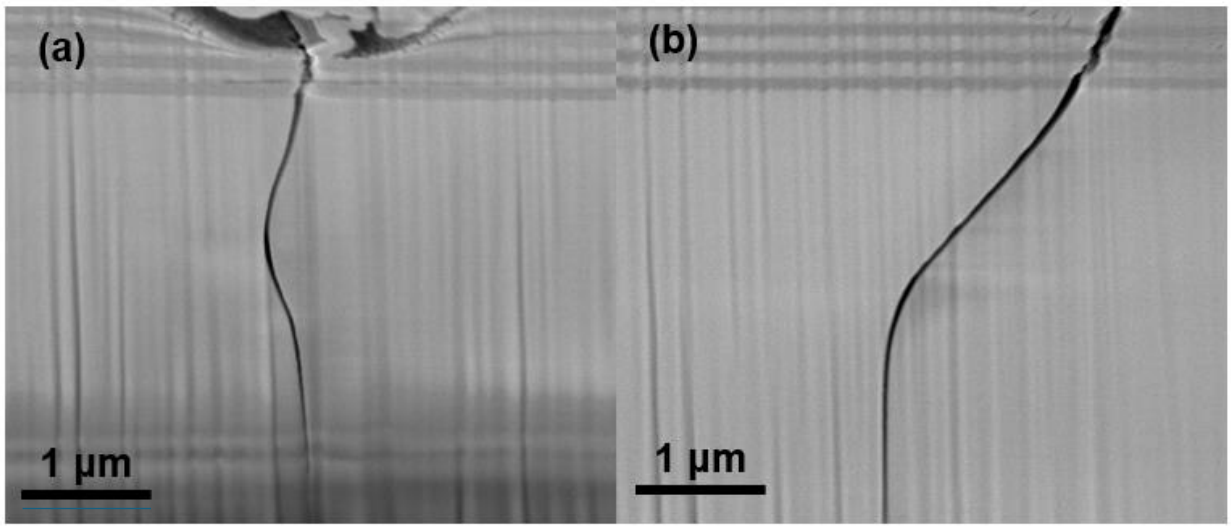

Fig. 4. Cracking was observed in the FIB micrographs for both locations studied. (a) corresponds to the area "1" in Fig. 2(a) and (b) corresponds to the area "2" in Fig. 2(a).

To the author's understanding, this is the first time that substrate cracking under nodular defects has been observed and documented for a brittle MLD coating on a brittle substrate. There are a few publications discussing the physics that would be required for stress in a brittle coating to drive a brittle substrate crack, but to date this is a novel experimental observation.[16, 30-34] Numerous studies have examined how nodular defects can act as electric field and stress concentrators in multilayer dielectric (MLD) high-reflector coatings under nanosecond laser irradiation, often leading to localized coating failure, delamination, or even substrate damage.[16, 30-37] While these works establish that nodular defects can lead to coating or substrate failure under laser irradiation, inducing crack initiation and propagation, they do not address the specific configuration observed here. Namely, a nodular defect within the MLD stack that induces cracking into a brittle substrate purely because of stress concentration from the MLD coating itself, without the aid of thermal or laser-induced excitation. Some previous studies have focused on how a brittle film under tensile stress can induce cracking in a ductile substrate.[38] In contrast, our system uses a brittle substrate (fused silica), where fracture proceeds without the plastic dissipation that governs ductile-substrate cracking. As a result, the energy-release rates, crack-spacing laws, and failure modes differ from the ductile case. Two relevant analogs were found in the literature. One is provided by the study of Poulingue et al.,[39] where controlled nodular defects were introduced at the interface between the aluminum substrate and the HfO_2/SiO_2 multilayer coatings. In the paper, the samples were tested under tensile stress, and they observed that cracks consistently initiated at nodular defect sites during the tensile stress tests. However, the authors only looked at the surface of the MLD stack. The estimated strain energy release rate for the multilayer stack was comparable to that of brittle materials like glass. The authors concluded that the nodular defects induced a local stress-raising effect that governs both the nucleation and propagation of coating cracks observed in the study. The second relevant paper is from Yves Leterrier, [40] which investigated the mechanical durability of nanoscale oxide coatings on compliant polymer substrates. Although the substrate in their work was ductile rather than brittle, the study clearly demonstrates that deposition-induced internal stresses, particularly in the presence of coating defects, can be sufficient to initiate coating cracking, without the need for external thermal or laser irradiation. The present work extends this concept to brittle substrates such as fused silica, where similar stress-driven cracking is observed, but in a

mechanically stiffer and more fracture-prone system. While Leterrier's study did not focus specifically on nodular defects or crack propagation into the substrate, the mechanisms they identified — stress amplification at defect sites and associated coating fracture — closely resemble aspects of the behavior we observe. To our knowledge, however, no previous study has reported crack propagation from a nodular defect in an MLD stack into a brittle substrate like fused silica, driven solely by intrinsic stress amplification during deposition. As developed, nodules are known to decrease the damage performance of any MLDs. Little is known from systematic studies about how coating cracks impact system performance. However, the impact of such a configuration — a nodule accompanied by a crack — on the damage threshold of the final optical system remains unclear. Indeed, crack formation in stressed optical multilayers, particularly around nodular defects, can act as a stress-relief mechanism, segmenting the film and dissipating stored elastic energy.[41, 42] While such cracks are typically viewed as precursors to failure,[26] they also reduce the local stress field, potentially mitigating further damage propagation.[41, 42] This stress discharge complicates the relationship between cracks and laser-induced damage: the presence of a crack may, paradoxically, lower the mechanical vulnerability of the surrounding film, making its overall impact on the damage threshold less straightforward.

3.2 Crack Initiation Hypothesis and Stress Analysis

Stress generation in an MLD coating stack arises from various intrinsic and extrinsic mechanisms during film growth, such as the formation of isolated atomic islands and the resulting grain boundary stresses, thermal stress due to the mismatch in thermal expansion between the substrate and the film, and nodule defects, which can also induce grain boundaries that contribute to internal stress.[43] This list is not exhaustive.

Using a fracture mechanics approach we can estimate the local stress concentration induced by the nodule.[44] Assuming an infinite plate geometry and that the observed crack length a = 5 μm (taken as the full length for a surface, which is much smaller than the substrate size of ~9 mm) governs the stress intensity, the mode I stress intensity factor is given by $K_I = \sigma_{local}\sqrt{\pi a}$. At the onset of crack propagation, this value is equal to the fracture toughness K_{IC} of fused silica — approximately 0.75 MPa·√m — which yields $\sigma_{local} \approx 189$ MPa.[45] This result indicates a local

stress concentration factor, $SCF = \sigma_{local}/\sigma_{nominal} \approx 1.18$, where $\sigma_{nominal}$ is the measured average tensile stress in the coating. This value can be calculated using the Stoney Equation with the change in surface figure of the substrate before and after coating via the interferometric reflected wavefront.[3, 4] The coating is observed to be tensile by approximately 160 MPa. This is the average value, and as mentioned above defects like nodules may significantly increase the local tensile stress state in the vicinity of the nodule, where local geometry and interfacial interactions can significantly alter the stress distribution.[46] Nonetheless, this analysis suggests that a modest amplification of coating stress at the nodular defect would have been sufficient to drive crack growth into the substrate up to the observed 5 μm extent, beyond which the stress intensity likely fell below the critical threshold for further propagation.

If the scenario involves a pre-existing fine surface crack in the substrate like those observed in sub-surface finishing damage, then Griffith's criterion should be able to explain crack initiation if the local coating stress alone is sufficient to propagate it and there is an initiating flaw.[47] Considering the likely and substantive increase in local stress near a nodule, it is highly likely that nodular defects initiate the observed craze lines.[44] If the nodule is included in the critical flaw size, this requires an initiating defect in the subsurface of the brittle substrate of approximately 200 nm, which is a reasonable length for sub-surface damage from the polishing process.[25, 26, 48] Historically, crazing like this has been observed in tensile coatings of similar stress when used for MLD gratings, which effectively introduce micron-sized deformations in the surface, similar to the nodule that is observed in this work.[8-12]

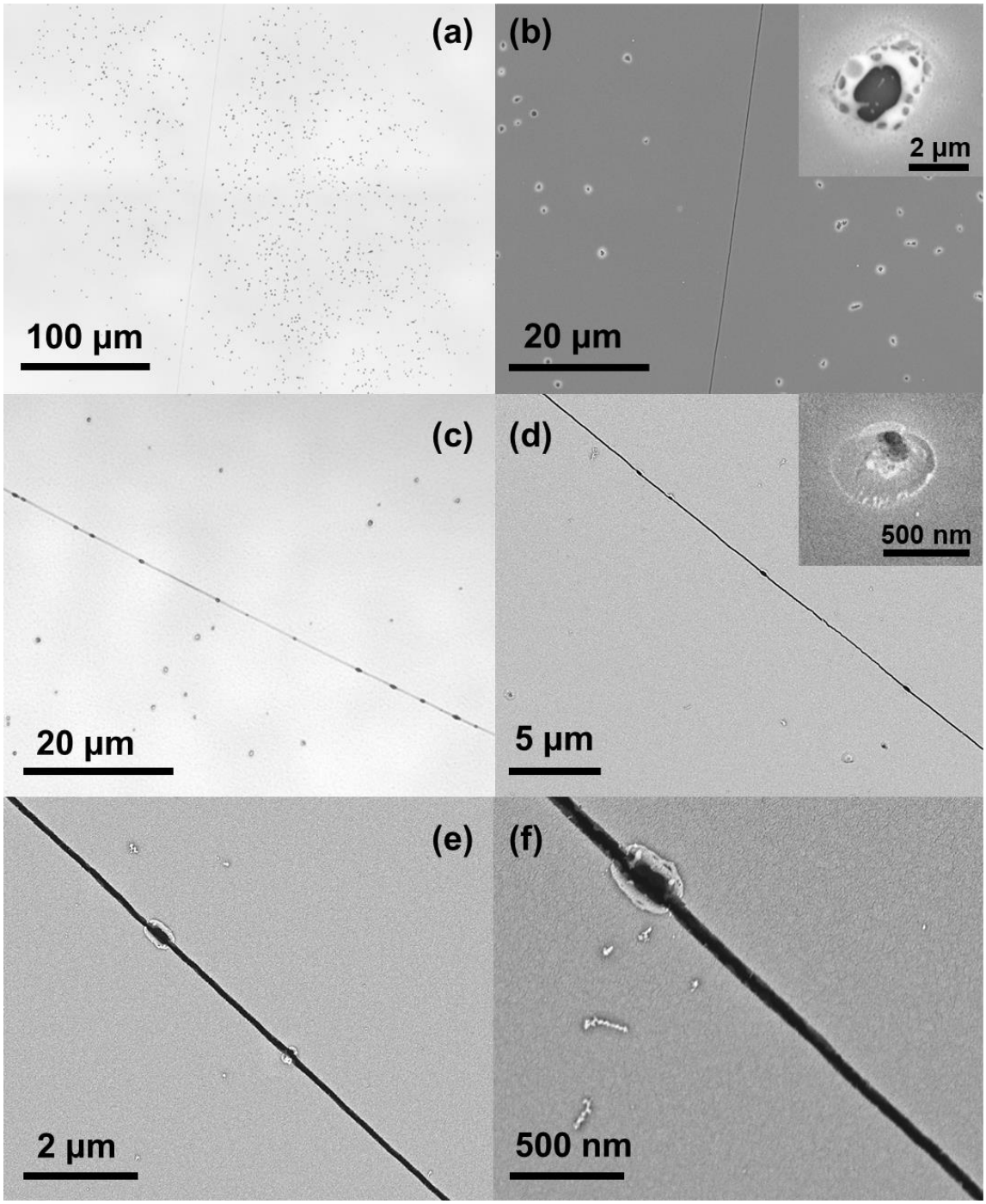

Fig. 5. Micrographs of laser-induced damage around the MLD craze lines: (a) confocal micrograph and (b) SEM micrograph at spot irradiation at 1064 nm (24 ± 2 J/cm²) along with an inset displaying the typical 1064 nm damage morphology; (c) confocal micrograph at spot irradiation at 355 nm (2.0 ± 0.2 J/cm²); (d) an SEM micrograph of damage spots along the craze lines visible in

(c) along with an inset displaying the typical 355 nm damage morphology; (e, f) zoomed in SEM micrographs of the damage in (d).

3.3 Nanosecond Laser Damage on craze lines at 1064 and 355 nm

When the sample is irradiated, there may be modifications to the pristine surface due to laser-matter interactions. This is a permanent change that is termed laser damage. Fig. 5 shows the laser-induced damage morphology on and near the MLD craze lines following irradiation at 1064 nm (24 ± 2 J/cm²; panels a and b) and 355 nm (2.0 ± 0.2 J/cm²; panels c–f), with laser confocal micrographs in panels a and c and SEM images in panels b, d–f. Fig. 5b and d have insets showing the typical 1064 and 355 nm laser damage morphology of damage away from the craze line. In the 1064 nm regime, we observe micron-sized damage pits with melted edges (Fig. 5b). This morphology is consistent with nano defect-driven, localized thermal damage in nanosecond pulses and is a common damage morphology for non-nodular initiated damage in an MLD at 1064 nm.[49, 50] At 355 nm, we see isolated damage pits lacking melted rims, reflecting ejection-like features, likely initiated by nano-precursors during nanosecond irradiation.[51] Again, this is a common damage morphology for 355 nm. The fluences for damage testing were selected so that they were just above the onset of laser damage for the pristine MLD coating at each wavelength. In the case of the 1064 nm irradiated sub-aperture, damage was observed on the pristine MLD surface but not on the craze line. This was observed at numerous fluences above the damage onset and in different sub-apertures on two different samples. This contrasts with the 355 nm irradiated sub-aperture where damage occurred occasionally on the pristine surface, but at high density along the craze line. Like the 1064 nm portion of this study, this was observed at numerous fluences above the damage onset and in multiple sub-apertures on two samples. As mentioned above, crazing has been observed in numerous transport mirrors and diffractive optics at long wavelengths and for large laser systems over the years and laser damage has not been observed on craze lines. [8-12] To our knowledge, this is the first reported observation directly linking UV laser damage with craze lines for MLDs coated with oxide materials. However, there is a large body of work linking scratches and fractures in dielectric oxide materials to UV laser damage.[25, 26] Crazing very likely leads to dangling oxide material bonds due to the craze line propagation similar to those seen in cracking and fracturing of bulk oxides. These defects are known to be less active for IR wavelengths but to be highly sensitive to UV wavelengths.[25,

27] The subtle eruption damage seen in Fig. 5f for the 355 nm laser damage on the craze line implies strongly that the damage is occurring high in the stack. Otherwise the damage morphology would look more similar to nodular ejection, where the damage initiates deeper in the structure and ejecting a high quantity of material.[52]

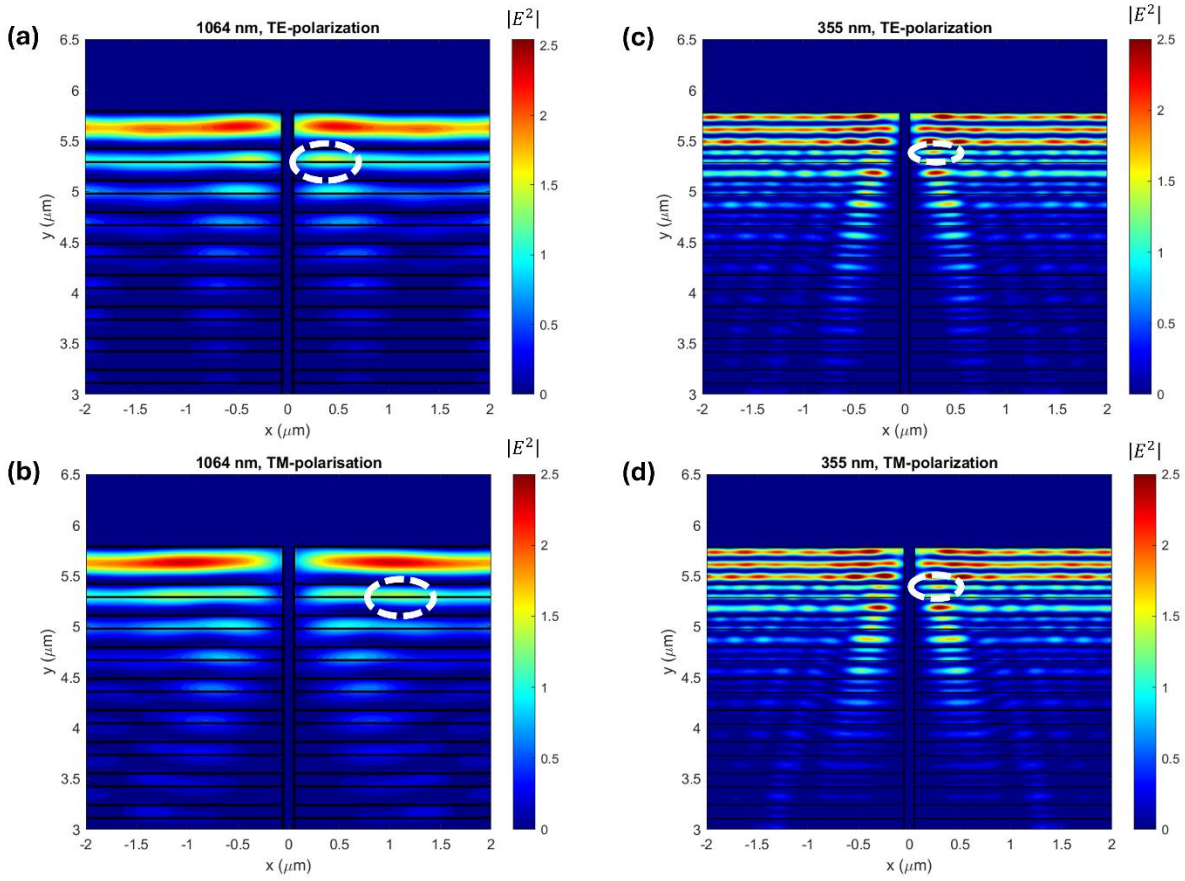

Fig. 6. Finite-difference time-domain simulations of the standing electronic field of the coating when irradiated at near-normal with a 100 nm craze line at (a) 1064 nm wavelength with T_E and (b) 1064 nm with T_M polarized light. (c, d) is for 355 nm wavelength and T_E and T_M polarized light respectively. The circled locations denote the highest electric field observed in the high index hafnia material.

3.4 Simulated electric field intensification induced by craze lines

The standing electric field in the vicinity of the 100 nm craze line was simulated for both wavelengths utilizing the Lumerical FDTD Maxwell equation solver, the results of which are in Fig. 6. The standing electric field at 1064 nm is largely insensitive to the 100 nm discontinuity, but when

simulated at 355 nm the electric field is amplified by approximately 3x. Fig. 6 shows the electric field distribution near the craze line for the 100 nm craze line width case. For the UV case, the 100 nm wide discontinuity is similar to the wavelength of light, making the scatter and light interaction with the craze line in the early Mie regime.[53] This leads to heavy forward scattering and electric field resonances as seen in electric field simulations of gratings and voids.[8, 9] This is seen in Fig. 6 (c, d) where there is a notable forward component to the modulation of the electric field due to the craze line discontinuity. When the wavelength of light is considerably longer than the perturbing feature, the resulting scatter is in the Rayleigh regime.[54] Unlike the Mie regime, the Rayleigh scattering regime has no directionality bias leading to scatter in all directions. This means that there is less forward propagation and less overall intensification in the coating stack. The 1064 nm case is more in the Rayleigh regime with less forward propagation as can be seen in Fig. 6 (a, b).

Numerous craze line widths were simulated and the maximal electric fields for the more damage-prone hafnia material are reported in Fig. 7 for both T_E and T_M polarization conditions. The top x-axis displays the width of the craze line simulated as a fraction of the wavelength used in the simulation. The line in each graph denotes the 100 nm width case observed in this study. As a validation check, the non-crazed sample condition was simulated and did not exhibit the periodicity observed in Fig. 6. This strongly suggests that there were no significant boundary condition impacts on the simulation. Unlike electric field simulations in bulk dielectric materials such as those from Bloembergen and Génin [5, 6], these simulations are for an MLD, where the design of the MLD can have large implications for the resultant electric fields. The simulations for the UV case do exhibit some notable electric field intensification when the wavelength is roughly equal to the craze line width, as predicted by Mie theory.[53] However, this effect is not seen in the IR case as strongly. There is some field intensification for the IR case when the craze line simulated is ~1000 nm wide, but it is minimal. This further emphasizes the importance of factoring in the MLD coating design when predicting phenomena like this.

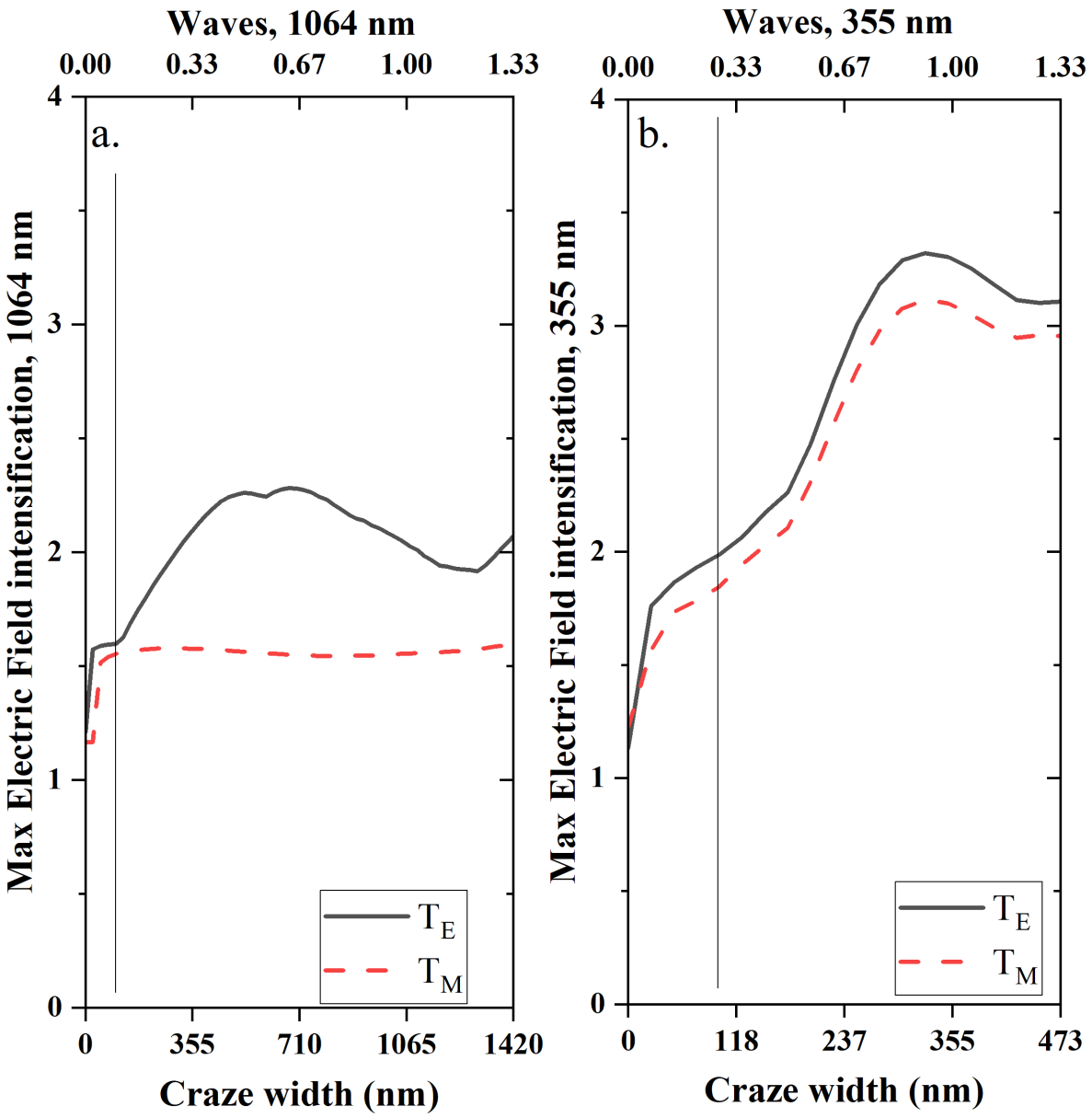

Fig. 7. Finite-difference time-domain simulations of the maximal electric field intensity for the high index hafnia material for (a) the 1064 nm and (b) the 355 nm case as a function of craze line thickness for both the T_E and T_M polarization conditions. The values are relative to the intensity of light input onto the MLD.

It has been previously shown that there is increased UV-sensitive defect density near cracks in dielectric materials.[25, 26, 28] It is notable that the increase in electric field is near where there is likely an increased defect density. These observations are similar to those observed and published

by Génin et al in their pivotal 2001 paper.[6] As shown in Fig. 6 for the 100 nm width craze line, the 1064 nm wavelength exhibits very little intensification. It is also notable that the intensification is observed to be near the interface between the two coating materials, where there are typically more damage-prone precursors in the form of dangling bonds and band-gap perturbation from material mixing. This intensification near material interfaces is common for quarter-wave based high-reflectors. While craze lines greater than 100 nm were not observed in this study, it may be possible if the coating stress is excessively high. The simulated values in excess of 100 nm are likely relevant to a crack or fracture in a surface, as discussed by Génin et al.[6]

4. Conclusion

This study presents observations suggesting a causal relationship between crazing appearance and/or propagation, and the presence of nodular defects. Under these nodular defects we observe long, 5 μm long cracks into the substrate which, to the author's knowledge, is a first of it's kind observation for a brittle-brittle system. This can be attributed to a pre-existing ~200 nm crack in the substrate due to sub-surface finishing damage and stress concentration induced by the nodule directly triggered crack propagation leading to cracking. We estimate that the stress concentration factor (SCF) of approximately 1.2 is needed for the nodule to induce a crack in the substrate as observed. The craze lines were irradiated with 1064 and 355 nm wavelength light at fluences slightly above the damage onset fluence. The areas irradiated with 1064 nm light had no damage initiation on the craze line, which is similar to the observations seen on MLD gratings for the ARC and HAPLS laser. However, when the craze lines were irradiated with 355 nm wavelength light, there were many damage sites that initiated on the craze line. This can be linked to a local increase in the electric field as simulated by FDTD in the vicinity of a region that has UV-sensitive defects. The field increase is attributed to the ~100 nm wide craze line being similar to the wavelength of light at 355 nm but much lower than the wavelength at the longer 1064 nm wavelength. The former leads to Mie scatter and resonance while the latter is in the Rayleigh scatter regime, leading to less forward propagation. This observation is consistent with similar simulations of similar phenomena and cracking in dielectric materials has long been linked to laser damage initiation and growth in at UV wavelengths.

Funding. Lawrence Livermore National Laboratory (23-ERD-006); U.S. Department of Energy (DE-AC52-07NA27344).

Acknowledgments. The authors would like to thank Eyal Feigenbaum and Hoang Nyguen for fruitful and insightful discussions.

Disclosures. The authors declare no conflicts of interest.

Data availability. Data presented in this paper may be obtained from the authors upon reasonable request.

References

1. J. Oliver, A. Rigatti, T. Noll, J. Spaulding, J. Hettrick, V. Gruschow, G. Mitchell, D. Sadowski, C. Smith, and B. Charles, "Large-aperture coatings for fusion-class laser systems" Applied Optics **59**, A7-A15 (2019).
2. H. Leplan, B. Geenen, J. Robic, and Y. Pauleau, "Residual stresses in evaporated silicon dioxide thin films: Correlation with deposition parameters and aging behavior" Journal of applied physics **78**, 962-968 (1995).
3. X. Feng, Y. Huang, and A. Rosakis, "On the Stoney formula for a thin film/substrate system with nonuniform substrate thickness" (2007).
4. G. G. Stoney, "The tension of metallic films deposited by electrolysis" Proceedings of the Royal Society of London. Series A, Containing Papers of a Mathematical and Physical Character **82**, 172-175 (1909).
5. N. Bloembergen, "Role of cracks, pores, and absorbing inclusions on laser induced damage threshold at surfaces of transparent dielectrics" Applied optics **12**, 661-664 (1973).
6. F. Y. Genin, A. Salleo, T. Pistor, and L. Chase, "Role of light intensification by cracks in optical breakdown on surfaces" Journal of the Optical Society of America A **18**, 2607-2616 (2001).
7. D. Strickland and G. Mourou, "Compression of amplified chirped optical pulses" Optics communications **55**, 447-449 (1985).
8. J. Britten, I. Jovanovic, W. Molander, M. Aasen, C. Brown, T. Carlson, C. Hoaglan, L. Jones, H. Nguyen, and J. Nissen, "Advanced dielectric grating technology for high-energy petawatt lasers," in *Conference on Lasers and Electro-Optics*, (Optica Publishing Group, 2005), JFB5.
9. J. Neauport, N. Bonod, S. Hocquet, S. Palmier, and G. Dupuy, "Mixed metal dielectric gratings for pulse compression" Optics Express **18**, 23776-23783 (2010).
10. H. Nguyen, J. Britten, T. Carlson, J. Nissen, L. Summers, C. Hoaglan, M. Aasen, J. Peterson, and I. Jovanovic, "Gratings for high-energy petawatt lasers," in *Laser-Induced Damage in Optical Materials: 2005*, (SPIE, 2006), 488-495.
11. T. Willemsen, U. Chaulagain, I. Havlíčková, S. Borneis, W. Ebert, H. Ehlers, M. Gauch, T. Groß, D. Kramer, and T. Laštovička, "Large area ion beam sputtered dielectric ultrafast mirrors for petawatt laser beamlines" Optics Express **30**, 6129-6141 (2022).
12. R. A. Negres, C. W. Carr, T. A. Laurence, K. Stanion, G. Guss, D. A. Cross, P. J. Wegner, and C. J. Stolz, "Laser-induced damage of intrinsic and extrinsic defects by picosecond pulses on multilayer dielectric coatings for petawatt-class lasers" Optical Engineering **56**, 011008-011008 (2017).

13. K. Manes, M. Spaeth, J. Adams, M. Bowers, J. Bude, C. Carr, A. Conder, D. Cross, S. Demos, and J. D. Nicola, "Damage mechanisms avoided or managed for NIF large optics" Fusion Science and Technology **69**, 146-249 (2016).
14. F. L. Ravizza, M. C. Nostrand, L. M. Kegelmeyer, R. A. Hawley, and M. A. Johnson, "Process for rapid detection of fratricidal defects on optics using linescan phase-differential imaging," in *Laser-Induced Damage in Optical Materials: 2009*, (SPIE, 2009), 454-464.
15. R. Chow, M. R. Kozlowski, G. E. Loomis, and F. Rainer, "Damage thresholds of fluoride multilayers at 355 nm," in *24th Annual Boulder Damage Symposium Proceedings--Laser-Induced Damage in Optical Materials: 1992*, (SPIE, 1993), 312-321.
16. J. DiJon, E. Quesnel, B. Rolland, P. Garrec, C. Pelle, and J. Hue, "High-damage-threshold fluoride UV mirrors made by ion-beam sputtering," in *Laser-Induced Damage in Optical Materials: 1997*, (SPIE, 1998), 406-416.
17. C. Hooker, J. Lister, K. Osvay, D. Sheerin, D. Emmony, and R. Cowell, "Pulse-length scaling of laser damage at 249 nm in oxide and fluoride multilayer coatings" Optics letters **18**, 944-946 (1993).
18. T. Izawa, N. Yamamura, R. Uchimura, S. Kimura, and T. Yakuoh, "Damage threshold of fluoride HR coatings at 352 nm," in *24th Annual Boulder Damage Symposium Proceedings--Laser-Induced Damage in Optical Materials: 1992*, (SPIE, 1993), 322-329.
19. X. Li, J. Liu, Y. Hou, K. He, W. Zhang, and K. Yi, "Improvement of the laser-induced damage threshold of oxide/fluoride double stack high reflective coatings at 355 nm by introducing interlayers" Applied surface science **280**, 772-775 (2013).
20. D. Smith and P. Baumeister, "Refractive index of some oxide and fluoride coating materials" Applied Optics **18**, 111-115 (1979).
21. T. Boehly, D. Brown, R. Craxton, R. Keck, J. Knauer, J. Kelly, T. Kessler, S. Kumpan, S. Loucks, and S. Letzring, "Initial performance results of the OMEGA laser system" Optics communications **133**, 495-506 (1997).
22. "Xcimer Energy Completes First Private-Sector Electron-Beam Excimer Laser" (2025), retrieved August 4, 2025, https://xcimer.energy/xcimer-energy-completes-first-private-sector-electron-beam-excimer-laser/.
23. C. J. Stolz, S. R. Qiu, R. A. Negres, I. L. Bass, P. E. Miller, D. A. Cross, J. A. Davis, S. Sommer, C. C. Widmayer, and B. J. MacGowan, "Transport mirror laser damage mitigation technologies on the National Ignition Facility," in *Advances in Optical Thin Films VI*, (SPIE, 2018), 82-93.
24. M. Poulingue, J. Dijon, M. Ignat, H. Leplan, and B. Pinot, "New approach for the critical size of nodular defects: the mechanical connection," in *Laser-Induced Damage in Optical Materials: 1998*, (SPIE, 1999), 370-381.
25. T. A. Laurence, J. D. Bude, N. Shen, T. Feldman, P. E. Miller, W. A. Steele, and T. Suratwala, "Metallic-like photoluminescence and absorption in fused silica surface flaws" Applied Physics Letters **94**, 151114 (2009).
26. T. A. Laurence, J. D. Bude, N. Shen, P. E. Miller, W. A. Steele, G. Guss, J. J. Adams, L. L. Wong, M. D. Feit, and T. I. Suratwala, "Ultrafast photoluminescence as a diagnostic for laser damage initiation," in *Laser-Induced Damage in Optical Materials: 2009*, (International Society for Optics and Photonics, 2009), 750416.
27. T. A. Laurence, J. D. Bude, N. Shen, W. A. Steele, and S. Ly, "Quasi-continuum photoluminescence: Unusual broad spectral and temporal characteristics found in defective surfaces of silica and other materials" Journal of Applied Physics **115**, 083501 (2014).

28. P. Miller, J. Bude, T. Suratwala, N. Shen, T. Laurence, W. Steele, J. Menapace, M. Feit, and L. Wong, "Fracture-induced subbandgap absorption as a precursor to optical damage on fused silica surfaces" Optics letters **35**, 2702-2704 (2010).
29. J. A. Pryatel, W. H. Gourdin, S. C. Frieders, G. S. Ruble, and M. V. Monticelli, "Cleaning practices and facilities for the National Ignition Facility (NIF)," in *Laser-Induced Damage in Optical Materials: 2014*, (SPIE, 2014), 390-410.
30. J. Dijon, M. Poulingue, and J. Hue, "Thermomechanical model of mirror laser damage at 1.06 um: I. Nodule ejection," in *Laser-Induced Damage in Optical Materials: 1998*, (SPIE, 1999), 387-397.
31. C. J. Stolz and E. Feigenbaum, "Temporal and spatial laser intensification within nodular defects overcoated with multilayer dielectric mirrors over a wide range of defect geometries" Applied Optics **62**, B25-B34 (2023).
32. G. Gatmaitan, C. J. Stolz, S. Diop, C. Harthcock, A. Guediche, E. Feigenbaum, T. Teklemarim, and M. Brophy, "High fluence oblique incidence low retardation multilayer dielectric mirror," in *Laser-Induced Damage in Optical Materials 2024*, (SPIE, 2024), 33-45.
33. X. Cheng, A. Tuniyazi, J. Zhang, T. Ding, H. Jiao, B. Ma, Z. Wei, H. Li, and Z. Wang, "Nanosecond laser-induced damage of nodular defects in dielectric multilayer mirrors" Applied optics **53**, A62-A69 (2014).
34. F. Bonneau, P. Combis, J.-L. Rullier, J. Vierne, B. Bertussi, M. Commandre, L. Gallais, J.-Y. Natoli, I. Bertron, and F. Malaise, "Numerical simulations for description of UV laser interaction with gold nanoparticles embedded in silica" Applied Physics B **78**, 447-452 (2004).
35. X. Cheng, J. Zhang, T. Ding, Z. Wei, H. Li, and Z. Wang, "The effect of an electric field on the thermomechanical damage of nodular defects in dielectric multilayer coatings irradiated by nanosecond laser pulses" Light: Science & Applications **2**, e80-e80 (2013).
36. X. Liu, Y. a. Zhao, Y. Gao, D. Li, G. Hu, M. Zhu, Z. Fan, and J. Shao, "Investigations on the catastrophic damage in multilayer dielectric films" Applied Optics **52**, 2194-2199 (2013).
37. Y. Shan, H. He, C. Wei, Y. Wang, and Y. a. Zhao, "Thermomechanical analysis of nodule damage in HfO2/SiO2 multilayer coatings" Chinese Optics Letters **9**, 103101 (2011).
38. T. Guo, L. Qiao, X. Pang, and A. A. Volinsky, "Brittle film-induced cracking of ductile substrates" Acta materialia **99**, 273-280 (2015).
39. M. Poulingue, M. Ignat, and J. Dijon, "The effects of particle pollution on the mechanical behaviour of multilayered systems" Thin solid films **348**, 215-221 (1999).
40. Y. Leterrier, "Durability of nanosized oxygen-barrier coatings on polymers" Progress in materials science **48**, 1-55 (2003).
41. R. Huang, J. Prevost, Z. Huang, and Z. Suo, "Channel-cracking of thin films with the extended finite element method" Engineering Fracture Mechanics **70**, 2513-2526 (2003).
42. I. B. Cheikh, G. Parry, D. Dalmas, R. Estevez, and J. Marthelot, "Analysis of the multi-cracking mechanism of brittle thin films on elastic-plastic substrates" International Journal of Solids and Structures **180**, 176-188 (2019).
43. A. R. Shugurov and A. V. Panin, "Mechanisms of stress generation in thin films and coatings" Technical Physics **65**, 1881-1904 (2020).
44. T. L. Anderson and T. L. Anderson, *Fracture mechanics: fundamentals and applications* (CRC press, 2005).
45. T. I. Suratwala, *Materials science and technology of optical fabrication* (John Wiley & Sons, 2018).

46. H. Liddell, K. Mehrotra, J. Lambropoulos, and S. Jacobs, "Fracture mechanics of delamination defects in multilayer dielectric coatings" Applied Optics **52**, 7689-7698 (2013).
47. A. A. Griffith, "VI. The phenomena of rupture and flow in solids" Philosophical transactions of the royal society of london. Series A, containing papers of a mathematical or physical character **221**, 163-198 (1921).
48. T. Suratwala, W. Steele, L. Wong, M. D. Feit, P. E. Miller, R. Dylla-Spears, N. Shen, and R. Desjardin, "Chemistry and formation of the Beilby layer during polishing of fused silica glass" Journal of the American Ceramic Society **98**, 2395-2402 (2015).
49. C. J. Stolz, F. Y. Genin, T. Reitter, N. E. Molau, R. P. Bevis, M. K. Von Gunten, D. J. Smith, and J. Anzellotti, "Effect of SiO2 overcoat thickness on laser damage morphology of HfO2/SiO2 Brewster's angle polarizers at 1064 nm," in *Laser-Induced Damage in Optical Materials: 1996*, (SPIE, 1997), 265-272.
50. H. Jiao, T. Ding, and Q. Zhang, "Comparative study of Laser induce damage of HfO2/SiO2 and TiO2/SiO2 mirrors at 1064 nm" Optics express **19**, 4059-4066 (2011).
51. Q. Zhou, P. Ma, F. Qiu, Y. Pu, Z. Qiao, L. Lv, M. Zhang, and J. Die, "Material ejection and layer peeling-off in HfO2/SiO2 thin-film beam splitters induced by 1ω and 3ω lasers" Optical Materials **125**, 111894 (2022).
52. H. Ma, X. Cheng, J. Zhang, H. Jiao, B. Ma, Y. Tang, Z. Wu, and Z. Wang, "Effect of boundary continuity on nanosecond laser damage of nodular defects in high-reflection coatings" Optics letters **42**, 478-481 (2017).
53. M. Hentschel, K. Koshelev, F. Sterl, S. Both, J. Karst, L. Shamsafar, T. Weiss, Y. Kivshar, and H. Giessen, "Dielectric Mie voids: confining light in air" Light: Science & Applications **12**, 3 (2023).
54. M. Reed and B. Simon, *III: scattering theory* (Elsevier, 1979), Vol. 3.